Dissipation analysis on a large strain thermo-elasto-viscoplastic model using the Finite Element Method

Péricles R. P. Carvalho[1], Rodolfo A. K. Sanches[1]

[1]*Dept. of Structural Engineering, São Carlos School of Engineering, University of São Paulo*
Av. Trab. São Carlense, 13566-590, São Carlos, São Paulo, Brazil
periclescarvalho@usp.br, rodolfo.sanches@usp.br

Abstract. We present a phenomenological large strain thermo-elasto-viscoplastic constitutive model using the multiplicative decomposition of the thermal, elastic and plastic deformation gradients. The laws of thermodynamics are used as basis to formulate the model and to obtain the heat equation, including the dissipation from the viscoplastic component. An isotropic expansion law in exponential form is used for the thermal part of the deformation, and a neo-Hookean model is used for the elastic part. Plasticity is considered based on the von Mises yield criterion with Perzyna model to account for the viscous behavior of the plastic component, Norton's law for the overstress function, and the Armstrong-Frederick model of kinematic hardening. For the numerical integration of the evolution laws, we employ an exponential map method that ensures the property of plastic incompressibility. The resulting constitutive model is applied in a position-based Finite Element framework to solve the mechanical problem. The thermal problem is also solved by the Finite Element Method, using temperatures as nodal parameters, and the thermo-mechanical coupling is performed as an iterative partitioned method. Finally, a representative numerical example is selected to show the characteristics of the constitutive model, with special focus on the heat generated due to plastic dissipation over different strain and stress rates.

Keywords: Dissipation, elasto-viscoplastic, thermodynamics, large strain

1 Introduction

The study of elasto-viscoplastic materials finds several applications in engineering, including, for instance, metal forming processes. In order to accurately model the mechanical behavior of these materials, it is important taking into account the energy dissipation and heat generated by their inelastic mechanisms, leading to thermally-coupled models. In this sense, we propose a large strain thermo-elasto-viscoplastic model using the multiplicative decomposition concept, and following a thermodynamics basis similar to works such as Carvalho et al. [1], Lion [2], Dettmer and Reese [3], Vujošević and Lubarda [4]. The model is then implemented into a numerical framework using the Finite Element Method [5, 6], and applied to a representative numerical example in order to show its constitutive properties and dissipative behavior.

2 Kinematics basis

Let us denote by $\mathbf{F}$ the deformation gradient from the initial to the deformed configuration of a body, by $\mathbf{C} = \mathbf{F}^T\mathbf{F}$ the right Cauchy-Green tensor, and by $J = \det\mathbf{F}$ the Jacobian. In order to account for large strain problems, we employ in this work the multiplicative decomposition of the deformation gradient. Similarly to Vujošević and Lubarda [4], we write $\mathbf{F} = \mathbf{F}_m\mathbf{F}_t$, where $\mathbf{F}_m$ and $\mathbf{F}_t$ are the mechanical and thermal deformation gradients, respectively. Considering a thermally isotropic material, we have $\mathbf{F}_t = \lambda_t\mathbf{I}$, where $\mathbf{I}$ is the identity tensor, and λ_t is a scalar representing the thermal stretch. For the mechanical part, we write $\mathbf{F}_m = \mathbf{F}_e\mathbf{F}_p$, where $\mathbf{F}_e$ and $\mathbf{F}_p$ are the elastic and plastic deformation gradients, respectively. Finally, following Lion [2], the plastic part can be written as $\mathbf{F}_p = \mathbf{F}_{p_e}\mathbf{F}_{p_i}$, where $\mathbf{F}_{p_e}$ and $\mathbf{F}_{p_i}$ are the plastic-elastic and plastic-inelastic deformation gradients, respectively. To summarize:

$$\mathbf{F} = \lambda_t \mathbf{F}_m = \lambda_t \mathbf{F}_e \mathbf{F}_p = \lambda_t \mathbf{F}_e \mathbf{F}_{p_e} \mathbf{F}_{p_i}. \tag{1}$$

For each given component of the deformation gradient, we can define respective components of the right Cauchy-Green tensor and Jacobian, e.g. $\mathbf{C}_e = \mathbf{F}_e^T \mathbf{F}_e$, $\mathbf{C}_{p_e} = \mathbf{F}_{p_e}^T \mathbf{F}_{p_e}$, $J_e = \det \mathbf{F}_e$ and $J_{p_e} = \det \mathbf{F}_{p_e}$.

3 Thermo-elasto-viscoplastic model

We base our model on the first and second laws of thermodynamics, written in a local Lagrangian form as

$$\dot{\psi} + T\dot{\eta} + \dot{T}\eta - R = \frac{1}{2}\,\mathbf{S} : \dot{\mathbf{C}} - \boldsymbol{\nabla}_0 \cdot \mathbf{q}_0, \text{ and} \tag{2}$$

$$d_{int} = \frac{1}{2}\,\mathbf{S} : \dot{\mathbf{C}} - \dot{\psi} - \dot{T}\eta - \frac{1}{T}\mathbf{q}_0 \cdot \boldsymbol{\nabla}_0 T \geq 0. \tag{3}$$

where ψ, η, R and d_{int} are the helmholtz free energy, entropy, internal heat, and dissipation rate, respectively, all defined per unit volume at the initial configuration, T the temperature, $\mathbf{S}$ the second Piola-Kirchhoff stress, $\mathbf{q}_0$ the heat flux in the initial configuration, and $\boldsymbol{\nabla}_0$ the gradient in the initial configuration.

Following Vujošević and Lubarda [4], the helmholtz free energy can be decomposed as $\psi = \lambda_t^3 \psi_m + \psi_t$, where ψ_m is the mechanical part, written in terms of the mechanical strain, and ψ_t is the thermal part, written in terms of the temperature. Furthermore, for the present elasto-viscoplastic model, the mechanical part can be decomposed as $\psi_m = \psi_e + \psi_{p_e}^{kin}$, where ψ_e is the elastic part, written in terms of the elastic strain, and $\psi_{p_e}^{kin}$ is the kinematic hardening part, written in terms of the plastic-elastic strain. Therefore, the helmholtz free energy can be expressed as

$$\psi(\mathbf{C}_e, \mathbf{C}_{p_e}, T) = \lambda_t^3 \psi_m(\mathbf{C}_e, \mathbf{C}_{p_e}) + \psi_t(T) = \lambda_t^3 \psi_e(\mathbf{C}_e) + \lambda_t^3 \psi_{p_e}^{kin}(\mathbf{C}_{p_e}) + \psi_t(T) \tag{4}$$

By applying eq. (4) into ineq. (3) and performing further algebraic manipulations using the multiplicative decomposition (section 2), we can express the second law of thermodynamics as

$$\begin{aligned} d_{int} = \; & \frac{1}{2}\left(\mathbf{S} - \lambda_t \mathbf{F}_p^{-1} \mathbf{S}_e \mathbf{F}_p^{-T}\right) : \dot{\mathbf{C}} + \lambda_t^3 \boldsymbol{\Sigma} : \text{Ł}_p + \lambda_t^3 \mathbf{M}_{p_e} : \text{Ł}_{p_i} \\ & - \left(\eta + \frac{\partial \psi_t}{\partial T} + 3\lambda_t^2 \psi_m \frac{\partial \lambda_t}{\partial T} - \lambda_t^2 \text{tr}\,\mathbf{M}_e \frac{\partial \lambda_t}{\partial T}\right) \dot{T} - \frac{1}{T}\mathbf{q}_0 \cdot \boldsymbol{\nabla}_0 T \geq 0, \end{aligned} \tag{5}$$

where $\text{Ł}_p = \dot{\mathbf{F}}_p \mathbf{F}_p^{-1}$ and $\text{Ł}_{p_i} = \dot{\mathbf{F}}_{p_i} \mathbf{F}_{p_i}^{-1}$ are the plastic and plastic-inelastic velocity gradients, respectively, $\mathbf{S}_e = 2\partial \psi_e / \partial \mathbf{C}_e$ is the elastic second Piola-Kirchhoff stress, $\boldsymbol{\Sigma} = \mathbf{M}_e - \mathbf{F}_{p_e} \mathbf{S}_{p_e} \mathbf{F}_{p_e}^T$ is called relative stress, $\mathbf{S}_{p_e} = 2\partial \psi_{p_e}^{kin} / \partial \mathbf{C}_{p_e}$ is the plastic-elastic second Piola-Kirchhoff stress, and $\mathbf{M}_e = \mathbf{C}_e \mathbf{S}_e$, $\mathbf{M}_{p_e} = \mathbf{C}_{p_e} \mathbf{S}_{p_e}$ are called Mandel stresses. From the arbitrarity of $\dot{\mathbf{C}}$ and $\dot{T}$, ineq. (5) leads to the following constitutive equations for the second Piola-Kirchhoff stress and the entropy:

$$\mathbf{S} = \lambda_t \mathbf{F}_p^{-1} \mathbf{S}_e \mathbf{F}_p^{-T}, \quad \text{and} \tag{6}$$

$$\eta = -\frac{\partial \psi_t}{\partial T} + \lambda_t^2 \left(\text{tr}\,\mathbf{M}_e - 3\psi_m\right) \frac{\partial \lambda_t}{\partial T}. \tag{7}$$

Additionally, following a Perzyna-like model [7] and an Armstrong-Frederick kinematic hardening [3], in order to guarantee the non-negativeness of the dissipation rate, the following evolution laws are applied:

$$\text{Ł}_p = \frac{\langle \Theta \rangle}{\eta_p} \frac{\boldsymbol{\Sigma}^D}{\|\boldsymbol{\Sigma}^D\|} \quad \Rightarrow \quad \dot{\mathbf{F}}_p = \frac{\langle \Theta \rangle}{\eta_p} \frac{\boldsymbol{\Sigma}^D}{\|\boldsymbol{\Sigma}^D\|} \mathbf{F}_p, \tag{8}$$

$$\text{Ł}_{p_i} = \frac{\langle \Theta \rangle}{\eta_p} \frac{b}{c} \mathbf{M}_{p_e}^D \quad \Rightarrow \quad \dot{\mathbf{F}}_{p_i} = \frac{\langle \Theta \rangle}{\eta_p} \frac{b}{c} \mathbf{M}_{p_e}^D \mathbf{F}_{p_i}, \tag{9}$$

where η_p is the plastic viscosity parameter, b and c are Armstrong-Frederick parameters (with c representing the kinematic hardening stiffness), $(\cdot)^D$ denotes the deviatoric tensor, $\|\cdot\|$ the tensor norm, $\langle\cdot\rangle$ the Macauley brackets, and Θ is the overstress. The latter is defined in this work by Norton's rule [8]: $\Theta = (\Phi/\alpha_p)^m$, where α_p and m are given parameters, and Φ is the yield function, considered here to be of von Mises type: $\Phi = \|\boldsymbol{\Sigma}^D\| - \sqrt{2/3}\,\sigma_Y$, with σ_Y being the yield stress.

By applying the constitutive relations and evolution laws above into the first and second laws of thermodynamics, we can express them as

$$d_m + R - c_p\dot{T} - \boldsymbol{\nabla}_0 \cdot \mathbf{q}_0 = 0, \quad \text{and} \tag{10}$$

$$d_{int} = d_m - \frac{1}{T}\mathbf{q}_0 \cdot \boldsymbol{\nabla}_0 T \geq 0, \tag{11}$$

where $c_p = T\,\partial\eta/\partial T$ is the specific heat capacity of the material (taken as a constant parameter in this work), and d_m is the mechanical part of the dissipation rate, in this case defined by the expression

$$d_m = \lambda_t^3 \frac{\langle\Theta\rangle}{\eta_p}\left(\|\boldsymbol{\Sigma}^D\| + \frac{b}{c}\|\mathbf{M}_{p_e}^D\|^2\right). \tag{12}$$

Equation (10) is also known as heat transfer equation, written in local Lagrangian form. As can be seen, the mechanical dissipation rate plays the same role of the internal heat, and, being always non-negative, it can only cause increases in temperature. The first law of thermodynamics also leads to the following relation:

$$\frac{1}{2}\,\mathbf{S} : \dot{\mathbf{C}} = \dot{\psi} + d_m + \dot{T}\eta, \tag{13}$$

that is, the internal work rate can be decomposed into three parts: the helmholtz free energy rate, the mechanical dissipation rate, and an entropy term.

4 Numerical implementation

The present constitutive model is applied into a position-based Finite Element framework [5, 6] for solving mechanical solid problems. To solve the heat transfer problem, we apply a temperature-based Finite Element method, using Fourier's law, which is written in Lagrangian form as $\mathbf{q}_0 = -kJ\mathbf{C}^{-1}\boldsymbol{\nabla}_0 T$, where k is the material conductivity parameter. For the thermal expansion, we apply the exponential law $\lambda_t = e^{\alpha(T-T_0)}$, where α is the thermal expansion coefficient and T_0 the reference temperature. The thermo-mechanical coupling is performed via an iterative partitioned method. For the mechanical parts of the helmholtz energy, we apply the following neo-Hookean laws:

$$\psi_e = \frac{\Lambda}{2}(\ln J_e)^2 + G\left(\operatorname{tr}\mathbf{C}_e - 3 - \ln J_e\right), \quad \text{and} \tag{14}$$

$$\psi_{p_e}^{kin} = \frac{c}{2}\left(\operatorname{tr}\mathbf{C}_{p_e} - 3 - \ln J_{p_e}\right). \tag{15}$$

where Λ and G are Lamé parameters, and c is the kinematic hardening stiffness. Finally, to numerically integrate the plastic and kinematic hardening evolution laws – eqs. (8) and (9) –, the exponential map method is used, which preserves the property of inelastic incompressibility [1].

4.1 Numerical example: partially loaded cube

To show the characteristics of the present formulation, we propose a partially loaded cube example, with geometry, mesh and material parameters shown in Fig. 1. This examples consists of monotonic loading and unloading stages, considering five different load rates: $75 \cdot 10^{-2}$, $75 \cdot 10^{-1}$, $75 \cdot 10^{0}$, $75 \cdot 10^{1}$ and $75 \cdot 10^{2}$ MPa/s. Furthermore, two different values of thermal expansion coefficients are considered: $\alpha = 0.003°\mathrm{C}^{-1}$ and $\alpha = 0.01°\mathrm{C}^{-1}$. The cube is treated as thermally sealed, that is, the generated heat does not dissolve into the environment, and the only heat source is the one generated by mechanical dissipation.

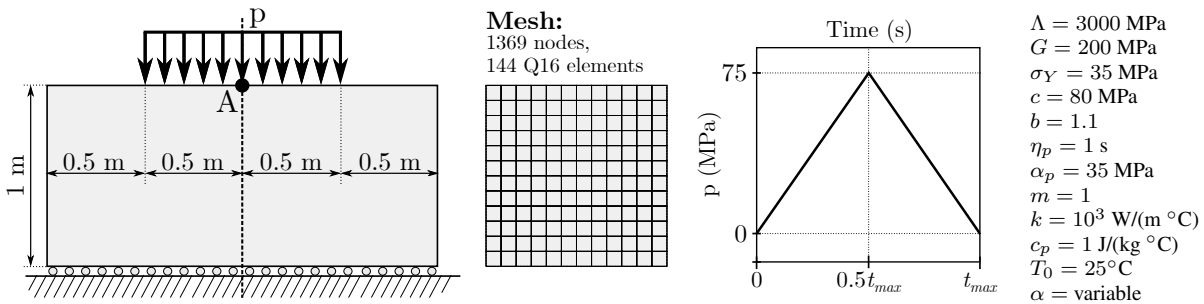

Figure 1. Geometry and parameters for the partially loaded cube example

In Fig. 2, we show the graphs of displacement over time for each of the different load rates and thermal expansion coefficients. As can be observed, the displacements are slightly smaller for the case with $\alpha = 0.01°C^{-1}$, and the effect of plastification is more significant as the loads rate decreases, tending to an hyperelastic behavior for higher load rate values. Furthermore, based on what is known of Perzyna-like models, we can also assume that the results for the lower load rates tend to a pure elasto-plastic model.

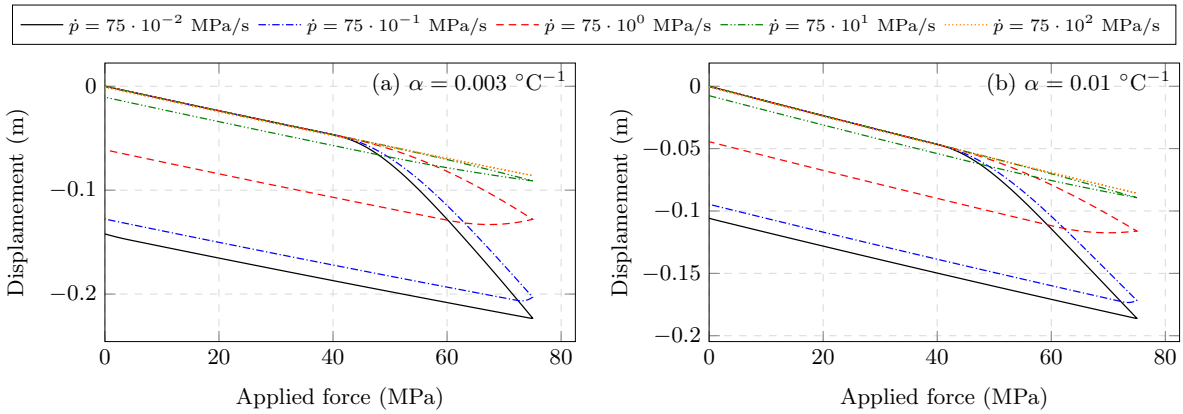

Figure 2. Displacement by force graphs for each analyzed case

In Fig. 3, we show a simple analysis of work rates for the case with $\alpha = 0.003$ °C^{-1}. The total external forces work rate is calculated by the expression $\int p\dot{\mathbf{y}}\, d\Gamma_p$, where p is the applied load in the boundary Γ_p, and $\dot{\mathbf{y}}$ is the displacement rate (velocity) of the points where the load is applied. Furthermore, we plot the values over time for each of the components of eq. (13), integrated over the initial volume, that is: total helmholtz rate (computed by a simple backward Euler approach), total mechanical dissipation rate, and an entropy term ($\int \eta\dot{T}\, dV_0$). By adding all these components to the total external forces work rate, we have the total mechanical work rate.

Proving the consistency of the present model, we note that the total mechanical work rate is approximately null in all cases, as expected from a closed system. From the presented graphs, it is also possible to have an idea of the dissipation magnitude for each case in comparison with the helmholtz rate. As can be seen, for higher load rates, the maximum mechanical dissipation rate becomes negligible relative to the other components, despite also increasing.

To allow a better visualization of the total mechanical dissipation rates (d_m) for each case, their graphs over time are shown individually in Fig. 4. Furthermore, in Fig. 5, we display the graphs of total mechanical dissipation for each case, which are calculated by integrating its rate over time (using a simple algorithm to get areas below the curve). We can observe that, although the total dissipation rate increases with the load rate, the total dissipation decreases. That is because the cases with higher load rates develop within a smaller time period, therefore reducing the integral over time value. This is expected, since the cases with lowest load rates are more influenced by the plasticity effect, which causes the dissipation.

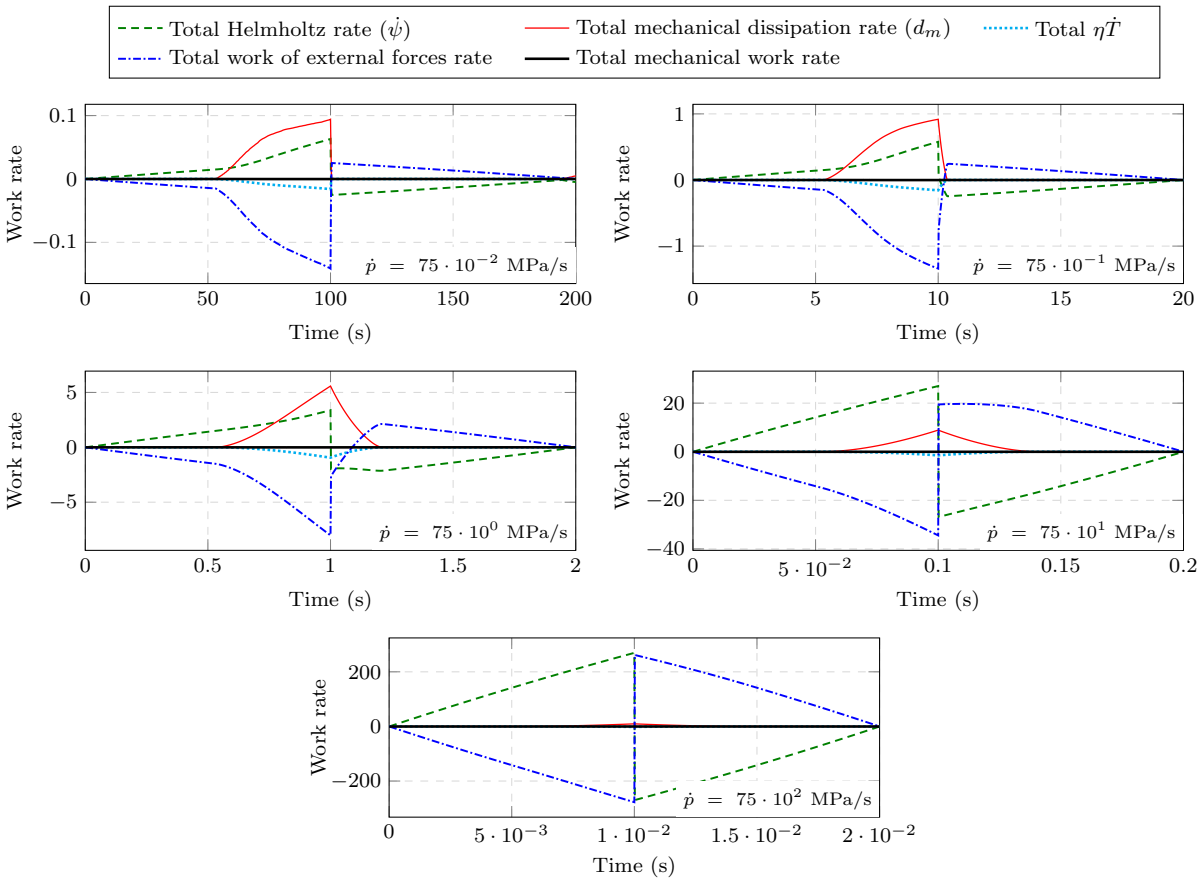

Figure 3. Work rates for the case with $\alpha = 0.003\ ^\circ\text{C}^{-1}$

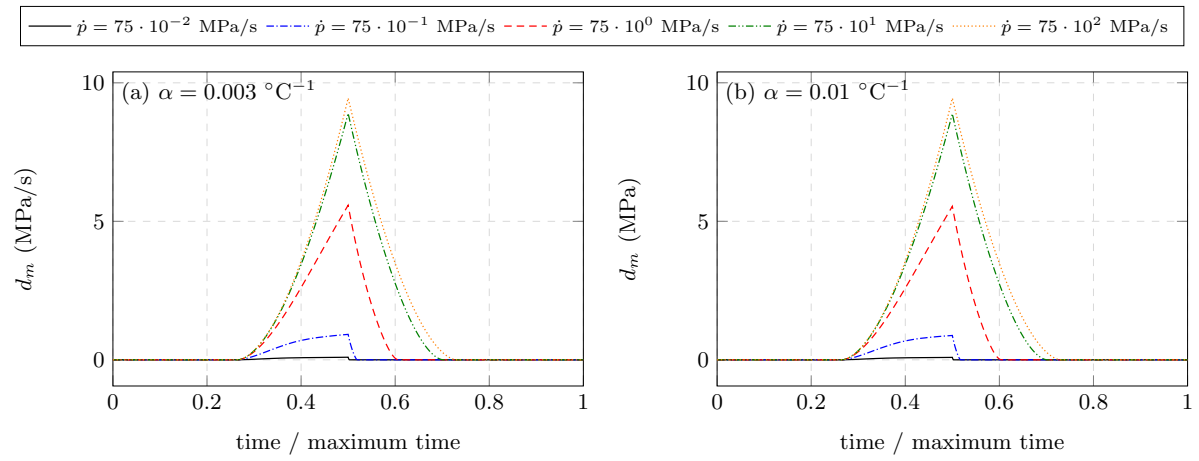

Figure 4. Total mechanical dissipation rate over time for each analyzed case

Finally, we show in Figs. 6 to 8 the deformed configurations of the present problem at the time with maximum load, particularly for the case with $\alpha = 0.003\ ^\circ\text{C}^{-1}$. Each figure presents a different variable in color map: vertical components of plastic deformation (Fig. 6), vertical components of Cauchy stress (Fig. 7), and temperatures (Fig. 8). As mentioned before, the plastic deformations increase – and become more localized – as the load rates decrease. Furthermore, as expected, we can note greater temperature increases for the cases with lower load

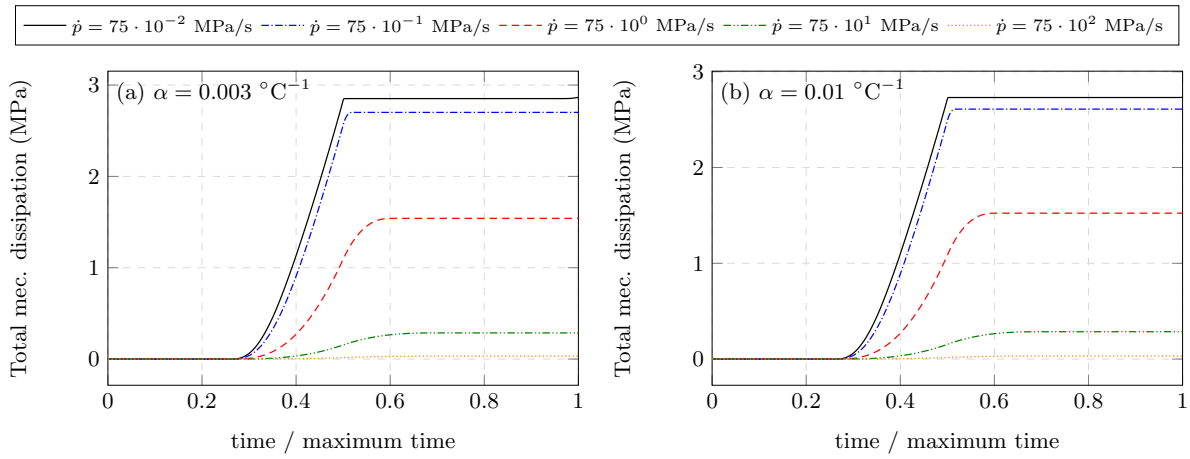

Figure 5. Total mechanical dissipation over time for each analyzed case

rates, despite the lower values of dissipation rates. Particularly for the case with $\dot{p} = 75 \cdot 10^{-2}$ MPa/s, we note an increase of approximately 2.85°C.

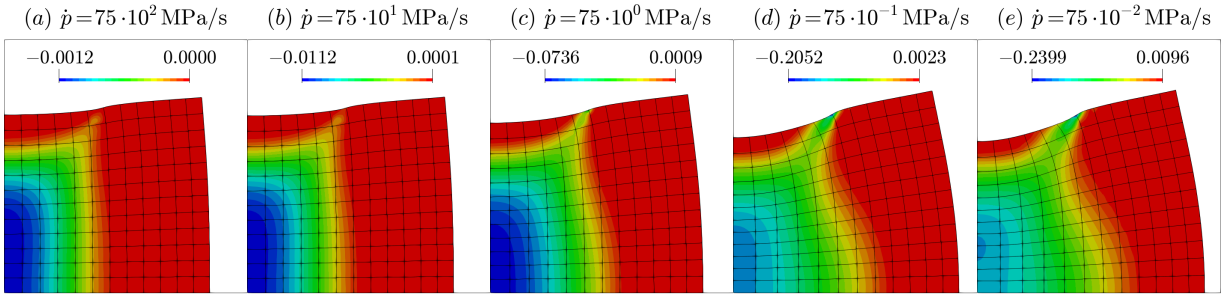

Figure 6. Deformed configurations at maximum load, with component $(E_p)_{22}$ displayed in color map

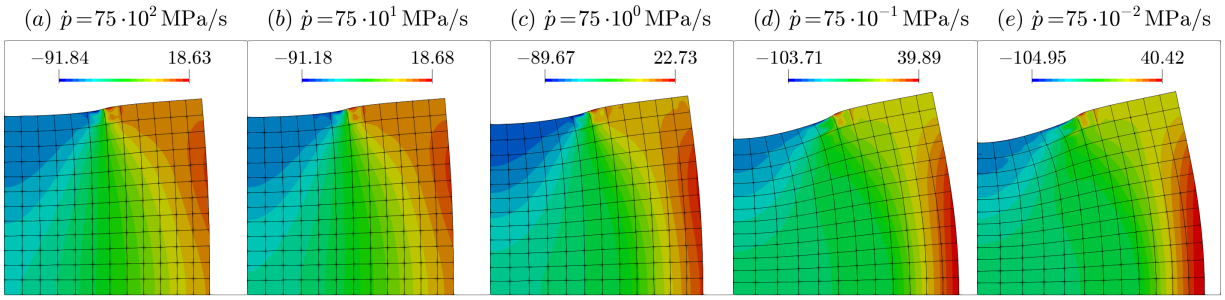

Figure 7. Deformed configurations at maximum load, with component σ_{22} displayed in color map

5 Conclusions

With the presented numerical example, we were able to display the behavior of the proposed thermo-elasto-viscoplastic model over a wide range of load rates, showing the rate-dependency of variables such as displacements,

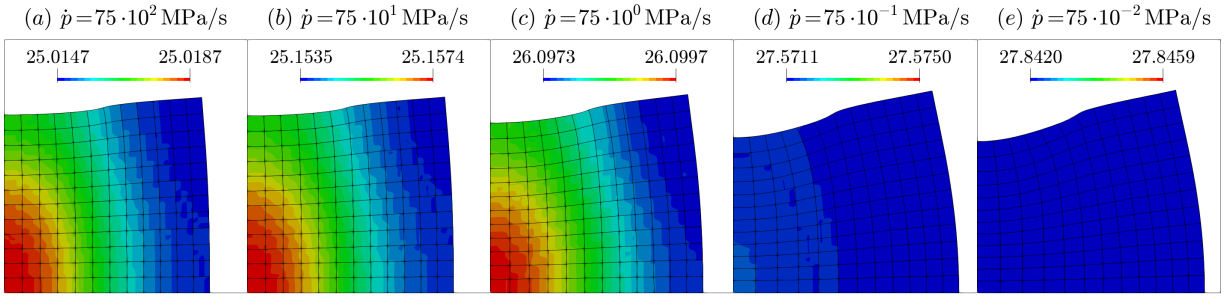

Figure 8. Deformed configurations at maximum load, with temperature displayed in color map

work rates, plastic strain, and total mechanical dissipation. In particular, the analysis of work rates allowed to prove the consistency of the present formulation, by showing that their components indeed balance each other. Furthermore, special focus was given to the total mechanical dissipation and its rate, including the influence of load rate on the temperature increase.

Acknowledgements. This study was financed in part by the *Coordenação de Aperfeiçoamento de Pessoal de Nível Superior – Brasil* (CAPES) – Finance Code 001 –, the Brazilian agency National Council for Scientific and Technological Development (CNPq) – grant 310482/2016-0 –, and the São Paulo Research Foundation (FAPESP) – Process Number 2018/23957-2. The authors would like to thank them for the financial support given to this research.

Authorship statement. The authors hereby confirm that they are the sole liable persons responsible for the authorship of this work, and that all material that has been herein included as part of the present paper is either the property (and authorship) of the authors, or has the permission of the owners to be included here.

References

[1] P. R. Carvalho, H. B. Coda, and R. A. Sanches. A large strain thermodynamically-based viscoelastic–viscoplastic model with application to finite element analysis of polytetrafluoroethylene (PTFE). *European Journal of Mechanics - A/Solids*, vol. 97, pp. 104850, 2023.
[2] A. Lion. Constitutive modelling in finite thermoviscoplasticity: a physical approach based on nonlinear rheological models. *International Journal of Plasticity*, vol. 16, n. 5, pp. 469 – 494, 2000.
[3] W. Dettmer and S. Reese. On the theoretical and numerical modelling of armstrong-frederick kinematic hardening in the finite strain regime. *Computer Methods in Applied Mechanics and Engineering*, vol. 193, n. 1, pp. 87 – 116, 2004.
[4] L. Vujošević and V. Lubarda. Finite-strain thermoelasticity based on multiplicative decomposition of deformation gradient. *Theoretical and applied mechanics*, , n. 28-29, pp. 379–399, 2002.
[5] H. B. Coda and R. R. Paccola. An alternative positional FEM formulation for geometrically non-linear analysis of shells: Curved triangular isoparametric elements. *Computational Mechanics*, vol. 40, n. 1, pp. 185–200, 2007.
[6] P. R. P. Carvalho, H. B. Coda, and R. A. K. Sanches. Positional finite element formulation for two-dimensional analysis of elasto-plastic solids with contact applied to cold forming processes simulation. *Journal of the Brazilian Society of Mechanical Sciences and Engineering*, vol. 42, n. 5, pp. 245, 2020.
[7] P. Perzyna. Fundamental problems in viscoplasticity. volume 9 of *Advances in Applied Mechanics*, pp. 243 – 377. Elsevier, 1966.
[8] J. J. Lemaitre. *Handbook of materials behavior models*. Academic Press, 2001.